

Fingerprints of the local moment formation and its Kondo screening in the generalized susceptibilities of many-electron problems

P. Chalupa^a, T. Schäfer^{b,c}, M. Reitner^a, S. Andergassen^d, and A. Toschi^a

^a*Institute of Solid State Physics, TU Wien, A-1040 Vienna, Austria*

^b*Collège de France, 11 place Marcelin Berthelot, 75005 Paris, France*

^c*CPHT, CNRS, École Polytechnique, IP Paris, F-91128 Palaiseau, France and*

^d*Institut für Theoretische Physik and Center for Quantum Science, Universität Tübingen, Auf der Morgenstelle 14, 72076 Tübingen, Germany*

(Dated: July 16, 2022)

We identify the precise hallmarks of the local magnetic moment formation and its Kondo screening in the frequency structure of the generalized charge susceptibility. The sharpness of our identification even pinpoints a novel criterion to determine the Kondo temperature of strongly correlated systems on the two-particle level, which only requires calculations at the *lowest* Matsubara frequency. We showcase its strength by applying it to the single impurity and the periodic Anderson model as well as to the Hubbard model. Our results represent a significant progress for the general understanding of quantum field theory at the two-particle level and allow for tracing the limits of the physics captured by perturbative approaches in correlated regimes.

Introduction. The goal of any successful theory is to extract essential features of the phenomena of interest from the complexity of the physical world, neglecting all superfluous pieces of information. This objective is particularly crucial for the cutting-edge quantum field theory (QFT) approaches designed to describe complex many-electron systems in the presence of strong correlations.

Presently, one can rely on a solid textbook interpretation[1, 2] of the QFT formalism describing the single-particle (1P) processes, measurable e.g. by the (angular resolved) direct and inverse photoemission[3] or the scanning tunneling microscopy[4, 5]. Crucial information about the metallic or insulating nature of a given many-electron problem, as well as quantitative information about the electronic mass renormalization Z and quasi-particle lifetime τ is unambiguously encoded in the momentum/energy dependence of the electronic self-energy Σ . If the temperature T is low enough, even a quick glance at the low-energy behavior of Σ , either in real or in Matsubara frequencies, can yield a qualitatively reliable estimate of the most important physical properties.

The situation is clearly very different on the two-particle (2P) level. Due to the higher complexity of the physical mechanisms at play, the related textbook knowledge is mostly limited to general definitions[1, 2]. For this reason corresponding analytical/numerical calculations are often performed with significant approximations or with a black-box treatment of the 2P processes. However, the last decade has seen a rapid development of methods at the forefront of the many-electron theory[6–8], for which generalized 2P correlations functions are the key ingredient. This is reflected in an increasing effort to develop the corresponding formal aspects and algorithmic procedures[6–20]. At the same time, our rather poor physical understanding of the 2P processes remains largely behind the requirements of the most advanced QFT methods. Interesting progress has been recently

reported[21, 22] on the relation of the 1P Fermi-liquid parameters to the scattering functions. Ideally, however, one would like to be able to interpret the physics encoded at the 2P level with a similar degree of confidence as for the 1P processes.

In our paper, we make a significant step forward in this direction: We identify the fingerprints of two major hallmarks of strong correlations in the generalized charge susceptibility. In particular, we pinpoint the frequency structures encoding the formation of local magnetic moments as well as of their Kondo screening. In this perspective, we also show how the Kondo temperature T_K corresponds to a specific property of the generalized charge susceptibility, allowing for an alternative, simple path of extracting its value directly from the lowest Matsubara frequency data.

We recall that the Kondo problem[24] provides a paradigm for a variety of physical effects involving strong electronic correlations, ranging from mesoscopic electron transport to heavy-fermion materials and high-temperature superconductors. In this work we focus on the formation of a local magnetic moment and its screening due to the interplay with a metallic surrounding, which can be described by effective Kondo problems, as it happens, e.g., in dynamical mean-field theory (DMFT)[25], with the auxiliary Anderson impurity model (AIM).

Learning how to extract physical information from the generalized susceptibility represents a substantial improvement for the understanding of quantum many electron physics at the 2P level. Further, having this information at hand also enables us to draw conclusions on two important theoretical questions: (i) The relation of the recently reported multifaceted manifestations[26] of the breakdown of perturbation theory, such as the divergences of the irreducible vertex functions[27–35] and the crossing of multiple solutions[26, 29, 33, 34, 36–38]

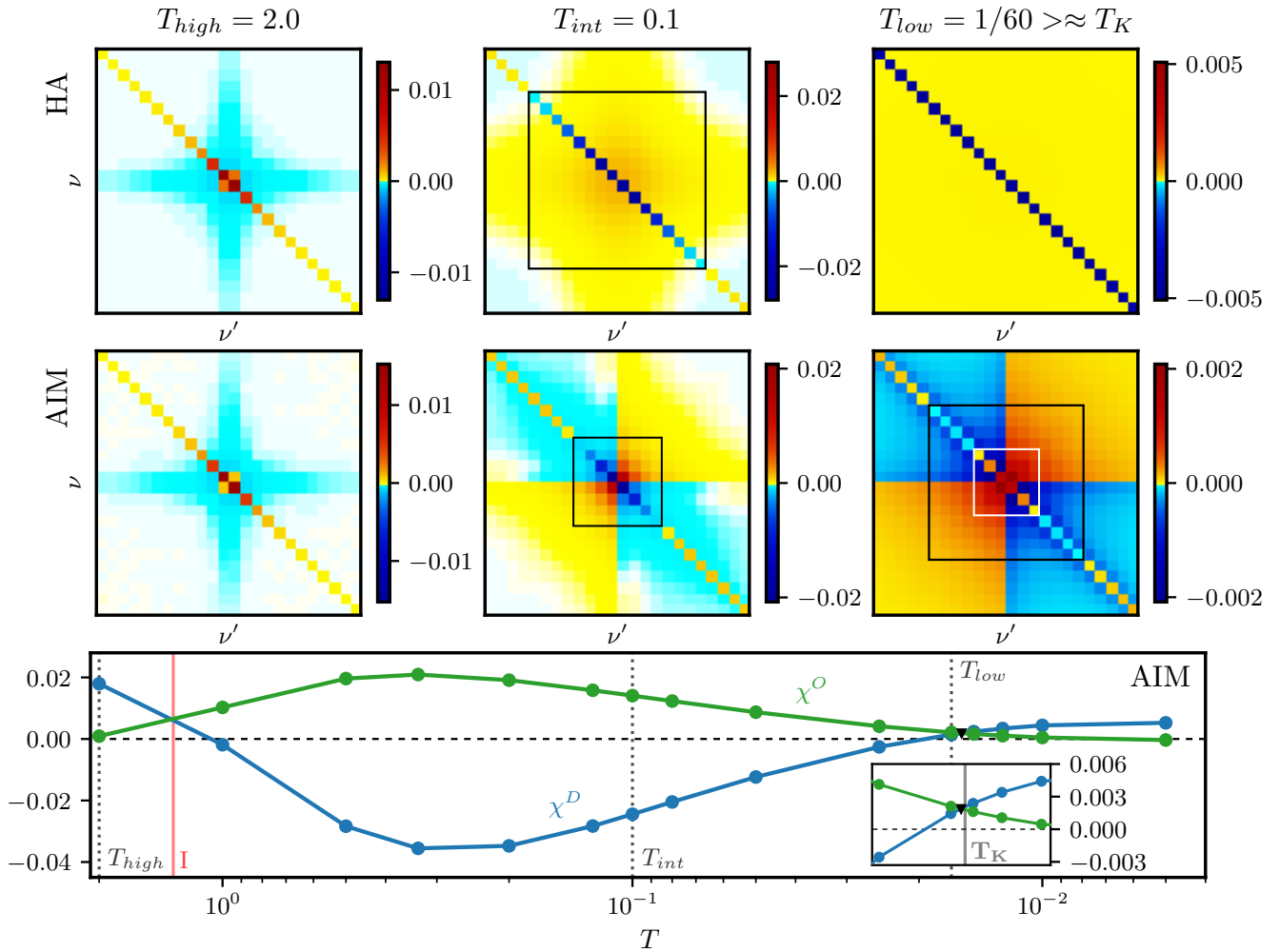


FIG. 1. Comparison of the Matsubara frequency structure of $T^2\chi^{\nu\nu'}(\Omega=0)$ for the HA (top) and the AIM (center) for $U=5.75$ and different temperatures. The maximal Matsubara index is kept fixed for all temperatures, and to ensure better readability the labels are hidden, see [23]. Black and white squares mark the main frequency structures, as described in the text. Lower panel: Temperature evolution of the lowest Matsubara frequency elements: $\chi^D = T^2\chi^{\pi T, \pi T}$ and $\chi^O = T^2\chi^{\pi T, -\pi T}$, crossing at T_{high} at the divergence of Γ (red (I)), and at low-temperatures at $T \simeq T_K$ (black triangle).

of the Luttinger-Ward functional, with the local moment physics and its Kondo screening; (ii) the built-in limit of advanced perturbative approaches to describe this kind of physics.

How to read two-particle quantities. We start from the definition of the generalized local susceptibility[10]

$$\chi_{\sigma\sigma'}^{\nu\nu'}(\Omega) = G_{\sigma\sigma'}^{(2)}(\nu, \nu', \Omega) - T^{-1}G(\nu)G(\nu')\delta_{\Omega 0}\delta_{\sigma\sigma'} \quad (1)$$

in terms of the 2P ($G^{(2)}$) and 1P (G) Green's functions, where ν, ν' and Ω are fermionic and bosonic Matsubara frequencies, and $\sigma, \sigma' = \{\uparrow, \downarrow\}$ spin indices. As we show in the following, for repulsive interactions, the generalized charge susceptibility $\chi^{\nu\nu'}(\Omega) = \chi_{\uparrow\uparrow}^{\nu\nu'}(\Omega) + \chi_{\uparrow\downarrow}^{\nu\nu'}(\Omega)$ allows for the best readability of the underlying physics at the 2P level. We recall that from the generalized susceptibility the physical response function can be readily

obtained by summing over the fermionic Matsubara frequencies: the static charge response $\chi(\Omega=0)$ is obtained in the following way

$$\chi = T^2 \sum_{\nu\nu'} \chi^{\nu\nu'} = T^2 \sum_{\nu\nu'} (\chi_{\uparrow\uparrow}^{\nu\nu'} + \chi_{\uparrow\downarrow}^{\nu\nu'}). \quad (2)$$

We first analyze the arguably simple case of an isolated atom with a repulsive interaction U (Hubbard atom, HA), where analytic expressions are available[10, 34]. In Fig. 1 (upper panels), we show an intensity plot of $\chi^{\nu\nu'}$ (normalized by T^2) for $U=5.75$, half filling (where $\chi^{\nu\nu'}$ is real) and different temperatures. At high temperature ($T_{\text{high}} = 2$, left panel), the overall frequency structure is dominated by a positive-valued diagonal (yellow/red). This corresponds to a typical *perturbative* behavior, dominated by the diagonal bubble term $\chi_0^{\nu\nu'} = -\delta_{\nu\nu'}G(\nu)^2/T$: Correlation effects are washed out

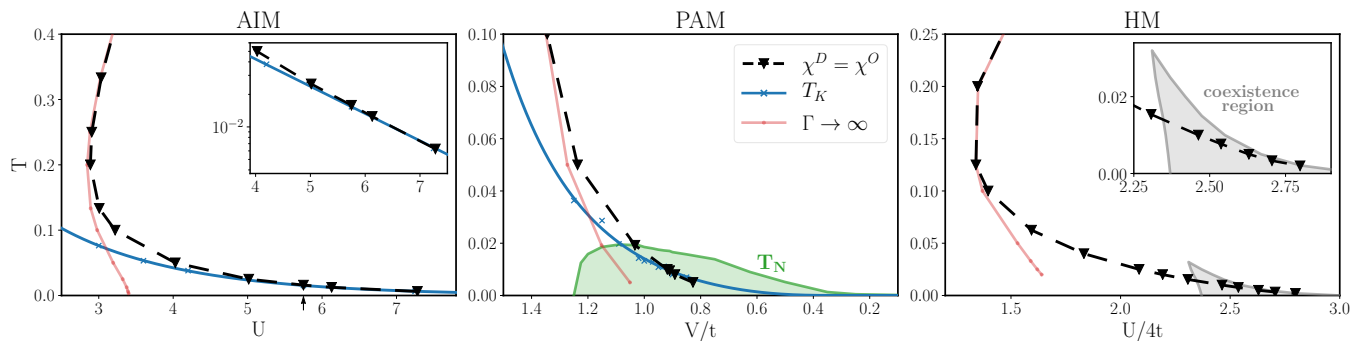


FIG. 2. Phase diagram of the AIM (left), the PAM (DMFT) (middle), and the HM (DMFT) (right) as a function of the interaction U (hybridization V for the PAM) and the temperature T . The left and central panel show the agreement at low temperatures between T_K (blue solid line) and the equality condition, i.e. the singularity of the 2×2 submatrix, $\chi^D = \chi^O$ (black triangles), clearly evident also in logarithmic scale (left inset). The red lines denote the (first) divergence of the irreducible vertex, the green area indicates the antiferromagnetic phase of the PAM and the coexistence region of the MIT of the HM on the Bethe lattice is shown in grey. The vertical arrow on the abscissa (left) marks the interaction value used in Fig. 1 and 3.

for $T \sim U$, consistently with the feasibility of high- T expansions.

The situation changes radically when reducing T : in the intermediate ($T_{\text{int}} = 0.1$) and low ($T_{\text{low}} = 1/60 \approx 0.017$) temperature regime (central and right panels), one observes a strong *damping* of all diagonal elements of $\chi^{\nu\nu'}$. The effect is more pronounced at low frequencies, as $\chi^{\nu\nu}$ becomes even *negative* (bluish colors) for $|\nu| \lesssim U$ [34] (black square). This major feature is accompanied by the appearance of *positive* off-diagonal elements (yellow), smaller in size w.r.t. the diagonal ones. The net effect is a suppression of the physical susceptibility, see Eq. (2), which occurs when the thermal energy is no longer large enough ($T \sim \nu < U$) to counter the formation of a local moment driven by U , eventually yielding and exponentially small $\chi \sim e^{-U/2T}$ for $T \rightarrow 0$. In fact, the low- T data of the HA (right panel) provides a perfect pedagogical illustration of how the onset of a “pure” local moment is encoded in the charge sector. Note that the progressive emergence of a sign structure in $\chi^{\nu\nu'}$, inverted w.r.t. the perturbative one, is responsible for all problematic manifestations[26] of the breakdown of perturbative expansions: The divergences[27–35] of irreducible vertex functions $\Gamma^{\nu\nu'} = [\chi^{\nu\nu'}]^{-1} - [\chi_0^{\nu\nu'}]^{-1}$, that directly reflect the sign changes of the eigenvalues of $\chi^{\nu\nu'}$, and the corresponding multivaluedness[26, 29, 33, 34, 36–38] of the Luttinger-Ward functional.

Let us now examine how this picture changes when the HA system is connected to an electronic bath (here: with a flat DOS of half bandwidth $D = 10$ and hybridization $V = 2 < U = 5.75$ [39]), corresponding to the well-known Anderson impurity model (AIM). By comparing the results of $T^2\chi^{\nu\nu'}$ (central-row panels of Fig. 1 computed with w2dynamics[40]) to those of the HA, we observe almost no difference at T_{high} . This is not surprising as thermal fluctuations prevail over both correlation (U) and hybridization (V) effects in this case. Lowering T

to T_{int} , we enter the *local moment* regime of the AIM. This is reflected in a qualitatively similar evolution as seen in the HA: a progressive suppression of the diagonal entries of $\chi^{\nu\nu'}$, becoming negative in the low-energy sector (black square), partly compensated by positive off-diagonal contributions. This is how the formation of a local moment affects the charge sector, suppressing local density fluctuations. Due to the screening effects of the bath, its action gets weakened, explaining the quantitative differences to the HA (e.g., the reduced size of the black square, and the less negative values on the diagonal, see [23] for a comparison).

The most interesting situation is observed by reducing T further down to $T_{\text{low}} \gtrsim T_K$ (right panel), where Kondo screening effects induce qualitative differences w.r.t. the HA. We clearly see that at low frequencies (white square) the sign of $\chi^{\nu\nu'}$ along the diagonal is flipped back to positive, similarly as in the perturbative regime. Physically, this nicely illustrates how the Kondo screening of the local moment acts *energy-selectively* in the charge sector, mitigating the suppression of density fluctuations at the lowest frequencies. Hence, the fingerprint of the Kondo regime is the *onion-like* frequency structure of $\chi^{\nu\nu'}$, which is clearly recognizable in the rightmost central panel of Fig. 1: (i) a high-frequency perturbative asymptotic, (ii) a local moment driven structure (with suppressed diagonal) at intermediate frequencies, (iii) an inner core (with a similar sign structure as (i)) induced by the Kondo screening. A quick glance at the overall sign structure of $\chi^{\nu\nu'}$ therefore allows for an immediate understanding of the underlying physics.

How to extract T_K . The behavior described above is also reflected in the temperature evolution of the lowest frequency entries of $\chi^{\nu\nu'}$: the diagonal $\chi^D = T^2\chi^{\pi T, \pi T}$ and the off-diagonal $\chi^O = T^2\chi^{\pi T, -\pi T}$, shown in the lowest panel of Fig. 1. Evidently, we can readily trace the sign changes marking the three regimes discussed above,

associating the (negative) minimum of χ^D with the temperature at which the strongest local moment effects are observed. The screening induced enhancement of χ^D at lower T has *remarkable consequences*: We find that crossing the Kondo temperature ($T_K = 1/65 \approx 0.015$ at $U = 5.75$ for the AIM[41]) matches, with high accuracy, the equality of χ^D and χ^O observed at low T (s. inset of Fig. 1, marked by black triangle). We emphasize that this criterion holds more generally. As shown in the phase diagram of the AIM in Fig. 2 (left panel), the condition $\chi^D = \chi^O$ (black triangles) traces perfectly T_K (blue line)[42] in the *whole* local moment regime $T, V < U$, i.e., where the definition of a Kondo scale is actually meaningful. Note that this is not the case for other criteria one could naturally think of, such as $\chi^D = -\chi^O$ or $\chi^D = 0$, see [23].

Moreover, our simple 2P definition of T_K holds also beyond the single impurity problem. In Fig. 2, we show DMFT calculations for the periodic Anderson model on a square lattice with nearest-neighboring hopping t (PAM, central) and for a Hubbard model on a Bethe lattice with unitary half-bandwidth (HM, right). We observe that for the PAM, the *same matching* of the condition $\chi^D = \chi^O$ (black triangles) and T_K [43, 44] (blue line) is found in the local moment regime (i.e., when $V < t$).

In the HM, the Kondo temperature characterizing the auxiliary AIM associated with the self-consistent DMFT solution, depends on the temperature itself: $T_K^{HM}(T)$. Hence, $\chi^D = \chi^O$ (black triangles) indicates that the temperature equals the effective Kondo temperature, i.e. $T_K^{HM}(T) = T$. Physically, it is natural to associate this condition to the onset of low-energy electronic coherence: For all temperatures below the $\chi^D = \chi^O$ condition line, a conventional Fermi-liquid behavior of the physical response is expected (e.g.: $\rho(T) \propto T^2, c_V(T) \propto T$, etc.[1]). This would be also consistent with the $\chi^D = \chi^O$ condition approaching the Mott Hubbard MIT at $U_{MIT}(T=0) = U_{c2}$ in the low- T limit (see also recent DMFT studies of the physics in the proximity of the MIT[45, 46]). The equality of the elements of the innermost 2×2 submatrix of $\chi^{\nu\nu'}$ represents therefore a very simple, clear-cut criterion for determining T_K at the 2P level.

A non-perturbative Fermi liquid. Beyond its physical relevance, our improved 2P understanding sheds light onto the nontrivial relation with the breakdown of perturbation theory[26]. At high T , where $\nu_0 = \pi T \gtrsim V, U, t$, the 2×2 submatrix encodes all relevant energy scales, the rest being nonsingular high-frequency asymptotics. In this case $\chi^D = \chi^O$ corresponds to a divergence of the *whole* $\chi^{\nu\nu'}$ and hence to a divergence of the irreducible vertex function $\Gamma^{\nu\nu'} = [\chi^{\nu\nu'}]^{-1} - [\chi_0^{\nu\nu'}]^{-1}$, specifically to the first (I) one encountered by increasing the interaction (red line in all plots)[27, 29, 32, 35]. At much lower temperatures $T \sim T_K$, one finds again $\chi^D > \chi^O$ as in the perturbative regime (s. Fig. 1, lowest panel). Here,

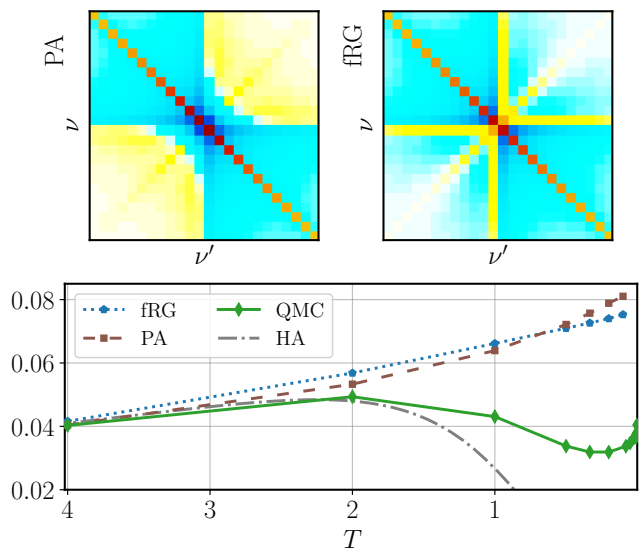


FIG. 3. Generalized charge susceptibility ($T^2 \chi^{\nu\nu'}$) for the AIM, as obtained from PA and fRG for $U = 5.75$ and $T = T_{int}$. The same color scale as in Fig. 1 (AIM, T_{int}) is used. The diagonal elements are all positive and the (positive) counter-diagonal structure is almost absent. Lower panel: static physical charge susceptibility χ in different approaches, where the numerically exact (QMC) displays the suppression due to local moment formation and the screening induced increase at low temperatures, both absent in the perturbative approaches (fRG, PA).

however, because of the onion-like structure of $\chi^{\nu\nu'}$, the positive-definiteness (and thus the invertibility) is guaranteed only for an inner submatrix describing the Fermi liquid regime, but not of the full $\chi^{\nu\nu'}$. This explains why divergences of irreducible vertex functions can occur also at low temperatures[32] even in the presence of a Fermi liquid ground state. Indeed, such vertex divergences mark the distinction between a Fermi liquid in the weak- and in the strong-coupling regime.

Limitations of perturbative approaches. The identification of the 2P fingerprints of local moments and their screening allows also to identify the limits to the physical description possible via perturbative approaches. As discussed above, the strong suppression of charge fluctuations in the local moment regime is encoded in negative diagonal and enhanced off-diagonal entries of $\chi^{\nu\nu'}$, which is associated[26] to several negative eigenvalues. Hence, the local moment physics, as well as its Kondo screening, cannot be accessed without crossing several divergences of Γ [29, 32]. This requirement is beyond perturbative approaches, where -per construction- Γ is finite[47]. We substantiate this statement by considering two of the most advanced perturbative schemes, the functional renormalization group (fRG)[48] and the parquet approximation (PA)[13, 49–55]. The results obtained for the AIM with $U = 5.75$ [56] and $T = T_{int}$ are shown in Fig. 3. $\chi^{\nu\nu'}$ computed by the fRG and PA ap-

pears qualitatively different from the (numerically) exact one of Fig. 1 (AIM, central): the diagonal elements are all *positive*, and substantially larger than the vanishing off-diagonal ones, see also [23]. This ensures the positive-definiteness of the whole $\chi^{\nu\nu'}$, ruling out, at the same time, the suppression effects of the charge response characterizing the local moment regime. This drawback qualitatively affects the physical description. In particular, the temperature dependence of the static susceptibility χ (Fig. 3 lower panel) exhibits a *clear minimum* for intermediate $T_K < T < T_{\text{high}}$. This emerges from the competition between the suppression effects of the local moment (see the extreme HA case) and the low-energy screening. Both features are not captured by the fRG and PA, which display a monotonous behavior.

Conclusions. We have shown how fundamental physical properties of correlated systems, i.e. the local moment formation and its Kondo screening, can be directly read in the Matsubara frequency structure of the generalized susceptibility $\chi^{\nu\nu'}$. In particular, the competition between localization effects and metallic screening are encoded in a clearly recognizable "onion-like" fingerprint in $\chi^{\nu\nu'}$, emerging in the Kondo regime. The thorough inspection of the latter even discloses an alternative, simpler, route to extract T_K directly from Matsubara frequency space. Eventually, our improved understanding of the 2P processes sets clear-cut limits to the physics accessible by means of perturbative approaches.

Acknowledgements - We thank M. Capone, S. Ciuchi, J. von Delft, K. Held, C. Hille, F. Krien, F.B. Kugler, and E. van Loon, G. Sangiovanni and D. Springer for insightful discussions. The authors also want to thank the Simons Foundation for hospitality. The present work was supported by the Austrian Science Fund (FWF) through the Project I 2794-N35 and Erwin-Schrödinger Fellowship J 4266 - "Superconductivity in the vicinity of Mott insulators" (SuMo, T.S.), the Deutsche Forschungsgemeinschaft (DFG) through Project No. AN 815/6-1, as well as the European Research Council for the European Union Seventh Framework Program (FP7/2007-2013) with ERC Grant No. 319286 (QMAC, T.S.).

[1] A. A. Abrikosov, L. P. Gorkov, and I. E. Dzyaloshinski, *Methods of Quantum Field Theory in Statistical Physics* (Dover, New York, 1975).
 [2] G. D. Mahan, *Many-Particle Physics* (Kluwer Academic/Plenum Publishers, New York, 2000).
 [3] A. Damascelli, Z. Hussain, and Z.-X. Shen, *Rev. Mod. Phys.* **75**, 473 (2003).
 [4] G. Binnig and H. Rohrer, *Rev. Mod. Phys.* **59**, 615 (1987).
 [5] O. Fischer, M. Kugler, I. Maggio-Aprile, C. Berthod, and

C. Renner, *Rev. Mod. Phys.* **79**, 353 (2007).
 [6] T. Maier, M. Jarrell, T. Pruschke, and M. H. Hettler, *Rev. Mod. Phys.* **77**, 1027 (2005).
 [7] W. Metzner, M. Salmhofer, C. Honerkamp, V. Meden, and K. Schönhammer, *Rev. Mod. Phys.* **84**, 299 (2012).
 [8] G. Rohringer, H. Hafermann, A. Toschi, A. A. Katantin, A. E. Antipov, M. I. Katsnelson, A. I. Lichtenstein, A. N. Rubtsov, and K. Held, *Rev. Mod. Phys.* **90**, 025003 (2018).
 [9] J. Kuneš, *Phys. Rev. B* **83**, 085102 (2011).
 [10] G. Rohringer, A. Valli, and A. Toschi, *Phys. Rev. B* **86**, 125114 (2012).
 [11] H. Hafermann, *Phys. Rev. B* **89**, 235128 (2014).
 [12] O. Gunnarsson, T. Schäfer, J. P. F. LeBlanc, E. Gull, J. Merino, G. Sangiovanni, G. Rohringer, and A. Toschi, *Phys. Rev. Lett.* **114**, 236402 (2015).
 [13] N. Wentzell, G. Li, A. Tagliavini, C. Taranto, G. Rohringer, K. Held, A. Toschi, and S. Andergassen, arXiv:1610.06520 (2016).
 [14] J. Kaufmann, P. Gunacker, and K. Held, *Phys. Rev. B* **96**, 035114 (2017).
 [15] A. Tagliavini, S. Hummel, N. Wentzell, S. Andergassen, A. Toschi, and G. Rohringer, *Phys. Rev. B* **97**, 235140 (2018).
 [16] E. G. C. P. van Loon, F. Krien, H. Hafermann, A. I. Lichtenstein, and M. I. Katsnelson, *Phys. Rev. B* **98**, 205148 (2018).
 [17] F. B. Kugler and J. von Delft, *Phys. Rev. B* **97**, 35162 (2018).
 [18] F. Krien, A. Valli, and M. Capone, *Phys. Rev. B* **100**, 155149 (2019).
 [19] E. G. C. P. van Loon and F. Krien, "The bethe-salpeter equation at the critical end-point of the mott transition," (2020), arXiv:2002.12745 [cond-mat.str-el].
 [20] M. Reitner, P. Chalupa, L. D. Re, D. Springer, S. Ciuchi, G. Sangiovanni, and A. Toschi, "Attractive effect of a strong electronic repulsion – the physics of vertex divergences," (2020), arXiv:2002.12869 [cond-mat.str-el].
 [21] F. Krien, E. G. C. P. van Loon, M. I. Katsnelson, A. I. Lichtenstein, and M. Capone, *Phys. Rev. B* **99**, 245128 (2019).
 [22] C. Melnick and G. Kotliar, "Fermi liquid theory and divergences of the two-particle irreducible vertex in the periodic anderson lattice," (2020), arXiv:2002.12904 [cond-mat.str-el].
 [23] See Supplemental Material available under ...
 [24] A. Hewson, *The Kondo Problem to Heavy Fermions* (Cambridge University Press, 1993).
 [25] A. Georges, G. Kotliar, W. Krauth, and M. J. Rozenberg, *Rev. Mod. Phys.* **68**, 13 (1996).
 [26] O. Gunnarsson, G. Rohringer, T. Schäfer, G. Sangiovanni, and A. Toschi, *Phys. Rev. Lett.* **119**, 056402 (2017).
 [27] T. Schäfer, G. Rohringer, O. Gunnarsson, S. Ciuchi, G. Sangiovanni, and A. Toschi, *Phys. Rev. Lett.* **110**, 246405 (2013).
 [28] V. Janiš and V. Pokorný, *Phys. Rev. B* **90**, 045143 (2014).
 [29] T. Schäfer, S. Ciuchi, M. Wallerberger, T. P., O. Gunnarsson, G. Sangiovanni, G. Rohringer, and A. Toschi, *Phys. Rev. B* **94**, 235108 (2016).
 [30] O. Gunnarsson, T. Schäfer, J. P. F. LeBlanc, J. Merino, G. Sangiovanni, G. Rohringer, and A. Toschi, *Phys. Rev. B* **93**, 245102 (2016).

- [31] T. Ribic, G. Rohringer, and K. Held, *Phys. Rev. B* **93**, 195105 (2016).
- [32] P. Chalupa, P. Gunacker, T. Schäfer, K. Held, and A. Toschi, *Phys. Rev. B* **97**, 245136 (2018).
- [33] J. Vučićević, N. Wentzell, M. Ferrero, and O. Parcollet, *Phys. Rev. B* **97**, 125141 (2018).
- [34] P. Thunström, O. Gunnarsson, S. Ciuchi, and G. Rohringer, *Phys. Rev. B* **98**, 235107 (2018).
- [35] D. Springer, P. Chalupa, S. Ciuchi, G. Sangiovanni, and A. Toschi, “Interplay between local response and vertex divergences in many-fermion systems with on-site attraction,” (2019), [arXiv:1912.02546 \[cond-mat.str-el\]](https://arxiv.org/abs/1912.02546).
- [36] E. Kozik, M. Ferrero, and A. Georges, *Phys. Rev. Lett.* **114**, 156402 (2015).
- [37] A. Stan, P. Romaniello, S. Rigamonti, L. Reining, and J. A. Berger, *New J. Phys.* **17**, 093045 (2015).
- [38] W. Tarantino, B. S. Mendoza, P. Romaniello, J. A. Berger, and L. Reining, *Journal of Physics: Condensed Matter* **30**, 135602 (2018).
- [39] For the AIM the interaction U is often put into reference with $\Delta = V^2 \pi \rho_0$, where in our case $\Delta = \pi/5$. Hence $U/\Delta \approx 9.15$.
- [40] Calculations of the 1P and 2P impurity Green’s functions have been performed with a CT-QMC algorithm[57] in the hybridization expansion, i.e. the w2dynamics code[58].
- [41] To extract the Kondo temperature we follow an approach presented in Ref. [59], which is also applied for the same model and parameters in the appendix B of Ref. [32].
- [42] For different interaction values T_K is extracted (blue crosses), and then a fit based on the analytical expression for T_K in the wide-band limit[24] ($A\sqrt{U\Delta} \exp(-B\frac{U}{\Delta} + C\frac{\Delta}{U})$) is used.
- [43] T. Schäfer, A. A. Katanin, M. Kitatani, A. Toschi, and K. Held, *Phys. Rev. Lett.* **122**, 227201 (2019).
- [44] G. Rohringer, A. Katanin, T. Schäfer, A. Hausoel, K. Held, and A. Toschi, github.com/ladderDGA (2018).
- [45] H. Terletska, J. Vučićević, D. Tanasković, and V. Dobrosavljević, *Phys. Rev. Lett.* **107**, 026401 (2011).
- [46] J. Vučićević, H. Terletska, D. Tanasković, and V. Dobrosavljević, *Phys. Rev. B* **88**, 075143 (2013).
- [47] With the only exception of second-order phase transitions to long-range ordered phases, which is not relevant here.
- [48] We use the one-loop flow equations for the self-energy and two-particle vertex, see Ref. 7 for a review. For the details of the implementation we refer to the Supplemental Material [23].
- [49] D. Sénéchal, A.-M. Tremblay, and C. Bourbonnais, eds., “Theoretical methods for strongly correlated electrons,” (Springer-Verlag New York Berlin Heidelberg, 2004) pp. 237–296.
- [50] S. X. Yang, H. Fotsos, J. Liu, T. A. Maier, K. Tomko, E. F. D’Azevedo, R. T. Scalettar, T. Pruschke, and M. Jarrell, *Phys. Rev. E* **80**, 046706 (2009).
- [51] K.-M. Tam, H. Fotsos, S.-X. Yang, T.-W. Lee, J. Moreno, J. Ramanujam, and M. Jarrell, *Phys. Rev. E* **87**, 013311 (2013).
- [52] A. Valli, T. Schäfer, P. Thunström, G. Rohringer, S. Andergassen, G. Sangiovanni, K. Held, and A. Toschi, *Phys. Rev. B* **91**, 115115 (2015).
- [53] G. Li, N. Wentzell, P. Pudleiner, P. Thunström, and K. Held, *Phys. Rev. B* **93**, 195134 (2016).
- [54] V. Janiš, P. Zalom, V. Pokorný, and A. Klíč, *Phys. Rev. B* **100**, 195114 (2019).
- [55] A. Kauch, P. Pudleiner, K. Astleithner, P. Thunström, T. Ribic, and K. Held, *Phys. Rev. Lett.* **124**, 047401 (2020).
- [56] The value of $U = 5.75$ ($U/\Delta \approx 9.15$) has been chosen in such a way that the local magnetic moment is already well defined, and at the same time is still accessible within PA and fRG in order to allow for a direct comparison to Fig. 1. Similar results are obtained for other values of U , see [23].
- [57] E. Gull, A. J. Millis, A. I. Lichtenstein, A. N. Rubtsov, M. Troyer, and P. Werner, *Rev. Mod. Phys.* **83**, 349 (2011).
- [58] M. Wallerberger, A. Hausoel, P. Gunacker, A. Kowalski, N. Parragh, F. Goth, K. Held, and G. Sangiovanni, *Computer Physics Communications* **235**, 388 (2019).
- [59] H. R. Krishna-murthy, J. W. Wilkins, and K. G. Wilson, *Phys. Rev. B* **21**, 1003 (1980).